Sensors and Materials, Vol. 35, No. 5 (2023) 1647–1657
MYU Tokyo

S & M 3277

Design and Analysis of an AC/DC Charger with High Power Factor and High Efficiency

Cheng-Tao Tsai* and Feng-Wei Peng

Department of Electrical Engineering, National Chin-Yi University of Technology, Taichung 41170, Taiwan

(Received January 7, 2023; accepted April 26, 2023)

Keywords: power factor correction, inductor-inductance-capacitor resonant converter, soft-switching

In this paper, an AC/DC charger with high power factor and high efficiency is proposed. The topology of the AC/DC charger makes use of an active power factor correction (PFC) circuit and a DC/DC half-bridge inductor-inductance-capacitor (LLC) resonant converter with high efficiency, which has the following advantages: (1) By incorporating a current-sensing circuit, a zero-current detection circuit, and an active PFC circuit in the front, the AC source can decrease harmonic currents. Therefore, the power factor of the proposed AC/DC charger can approach 0.997. (2) By incorporating a DC/DC half-bridge LLC resonant converter with soft-switching functions in the rear, the power losses of the active switches can be decreased and the efficiency can be improved significantly. Finally, a prototype of the AC/DC charger with high power factor and high efficiency is designed and analyzed. The results of the experiments are presented to prove the function and probability of the AC/DC charger with high power factor and high efficiency.

1. Introduction

With the increasing awareness of air pollution and the importance of healthy leisure activities, electric bicycles (e-bikes) and electric motorcycles are becoming increasingly popular. E-bikes and electric motorcycles have the following advantages: (1) They do not cause air pollution problems. In cities, personal transportation can be replaced by e-bikes and electric motorcycles, so the problems of air pollution and traffic congestion can be significantly addressed. This will also improve the quality of people's life and health. (2) Green energy issues have become topics of concern worldwide. In the future, high-performance batteries, motor technologies, and power management systems incorporated with sensors, Internet of Things, a global positioning system, and safety protection will be applied to e-bikes and electric motorcycles.(1) Therefore, people and e-bikes as well as electric motorcycles can be connected more closely.(2)

There are two main types of important equipment in e-bikes and electric motorcycles: DC brushless motors and lithium ferrous phosphate (LFP) batteries. LFP batteries need an AC/DC charger for charging power energy.(3) Currently, AC/DC chargers with high power factor and high efficiency are required in the consumers' market. Therefore, AC/DC chargers with

*Corresponding author: e-mail: cttsai@ncut.edu.tw
https://doi.org/10.18494/SAM4307

ISSN 0914-4935

functions of low current harmonics and switching losses to increase the power factor and efficiency are necessary. In this paper, an AC/DC charger with high power factor and high efficiency is studied, and its structure is shown in Fig. 1. The AC/DC charger with high power factor and high efficiency consists of two stages. In the front stage, there is an AC/DC active power factor correction (PFC) circuit, as shown in Fig. 2. To increase the power factor of the AC/DC charger, the active PFC circuit is connected to a current-sensing circuit. When a zero-current signal of AC sources is sensed via the current-sensing circuit, a driving signal is delivered to turn on the power switch of the active PFC circuit. Thus, the distortion currents of AC sources are corrected to increase power factors.[4–7] In the rear stage, there is a DC/DC half-bridge inductor-inductance-capacitor (LLC) resonant converter with high efficiency, as shown in Fig. 3. To achieve the objectives of electrical isolation, high efficiency, high power, and low harmonic current of the AC/DC charger, a half-bridge LLC resonant circuit is selected in the DC/DC converter. This circuit has the advantages of a simple structure and electrical isolation.[8–11] Additionally, the power switches (M_1 and M_2) of the half-bridge LLC resonant circuit can be operated under soft-switching conditions during turn-on and turn-off transitions. Therefore, the switching losses of the power switches can be decreased and the efficiency of the DC/DC converter can be improved.[12–16] The overall circuit of the AC/DC charger with high power factor and high efficiency is shown in Fig. 4.

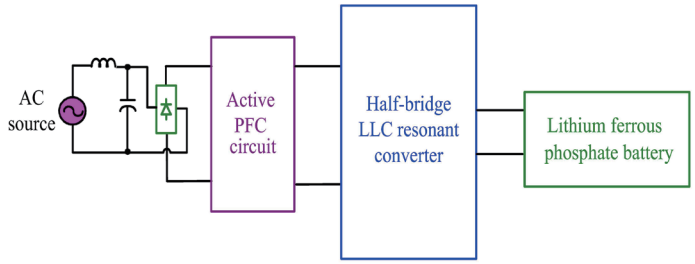

Fig. 1. (Color online) Structure of proposed AC/DC charger with high power factor and high efficiency.

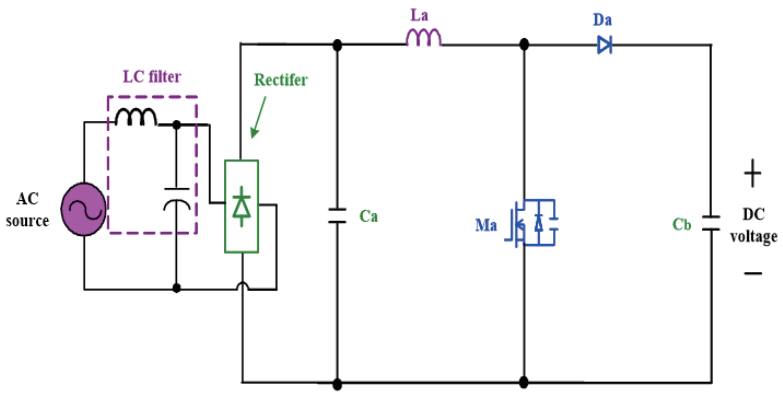

Fig. 2. (Color online) AC/DC active PFC circuit.

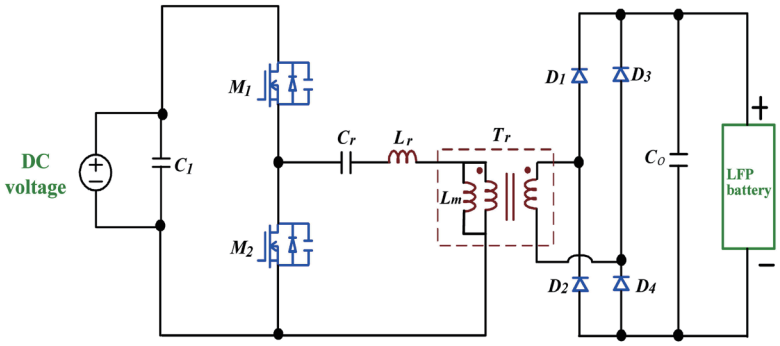

Fig. 3. (Color online) High-efficiency DC/DC half-bridge LLC resonant converter.

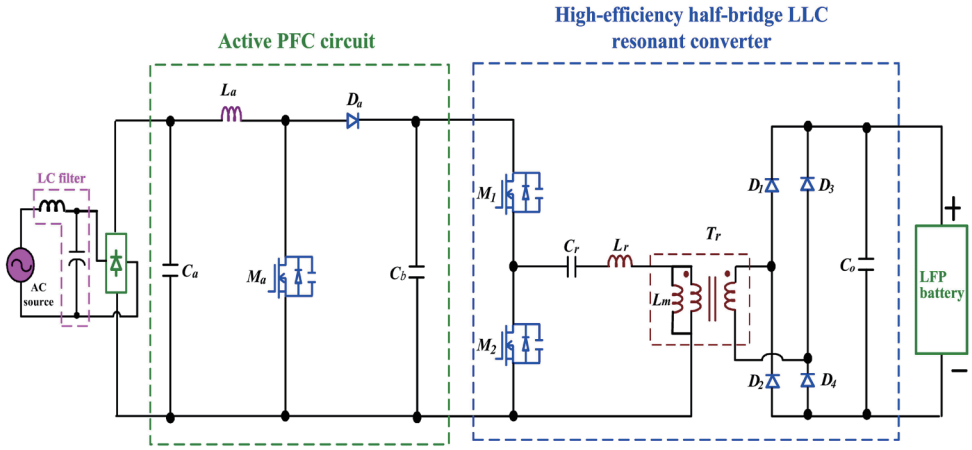

Fig. 4. (Color online) Overall circuit of AC/DC charger with high power factor and high efficiency.

The operational principles of the AC/DC charger with PFC and high efficiency are discussed in Sect. 2. The results of the experiments obtained from a prototype of the AC/DC charger with high power factor and high efficiency are shown in Sect. 3. Finally, conclusions are given in Sect. 4.

2. Operational Principles of AC/DC Charger with High Power Factor and High Efficiency

In this section, the operational principles of the AC/DC charger with high power factor and high efficiency are analyzed. There are two stages in the proposed AC/DC charger. In the front stage, there is an AC/DC PFC circuit. In the rear stage, there is a DC/DC half-bridge LLC resonant circuit. The operational principles of the AC/DC charger with high power factor and high efficiency can be divided into seven modes described as follows.

2.1 Operational Mode 1

While the power switch (M_a) of the AC/DC charger is turned off, the current i_{La} of the inductor (L_a) is linearly decreased. The active switch (M_1) is turned on and the power switch (M_2) is turned off. The energy stored in the inductor (L_a) is discharged and the magnetic inductance (L_m) of the transformer (T_r) is excited. The current i_{La} is flowing through the primary side of the transformer (T_r) $D_a \rightarrow M_1 \rightarrow C_r \rightarrow L_r \rightarrow L_m \rightarrow V_s$. In the secondary side of the transformer (T_r), the power diodes (D_3 and D_6) are switched on and the power diodes (D_4 and D_5) are switched off. The current i_{Lb} is flowing through the path $D_1 \rightarrow LFP$ battery$\rightarrow D_4$.

During this operational interval, the input current of the AC source equals the current i_{La} of the inductor (L_a). Therefore, the distorted currents of the AC source are corrected and the high power factor of the AC/DC charger is obtained. Figure 5 shows the equivalent circuit of the operational Mode 1.

2.2 Operational Mode 2

When the power switch (M_a) is continuously turned off and the power switches (M_1 and M_2) are turned off, the energy stored in the resonant inductor (L_r) is discharged. The parasitic capacitance (C_1) of the power switch (M_1) is charged and the parasitic capacitance (C_2) of the power switch (M_2) is discharged. The current i_{La} is flowing through the primary side of the transformer (T_r), which can be divided into two paths. One is $D_a \rightarrow C_1 \rightarrow C_r \rightarrow L_r \rightarrow L_m \rightarrow V_s$ and the other is $M_2 \rightarrow C_r \rightarrow L_r \rightarrow L_m$. In the secondary side of the transformer (T_r), the power diodes (D_3, D_4, D_5, and D_6) are turned off and the current i_{Lb} is flowing through the path $C_o \rightarrow LFP$ battery.

During this operational interval, the current i_{La} of the inductor (L_a) is linearly reduced. Figure 6 shows the equivalent circuit of the operational Mode 2.

2.3 Operational Mode 3

When the power switch (M_a) of the AC/DC charger is turned on and the current i_{La} of the inductor is linearly increased, the current i_{La} is flowing through the path $D_a \rightarrow M_a \rightarrow V_s$. The

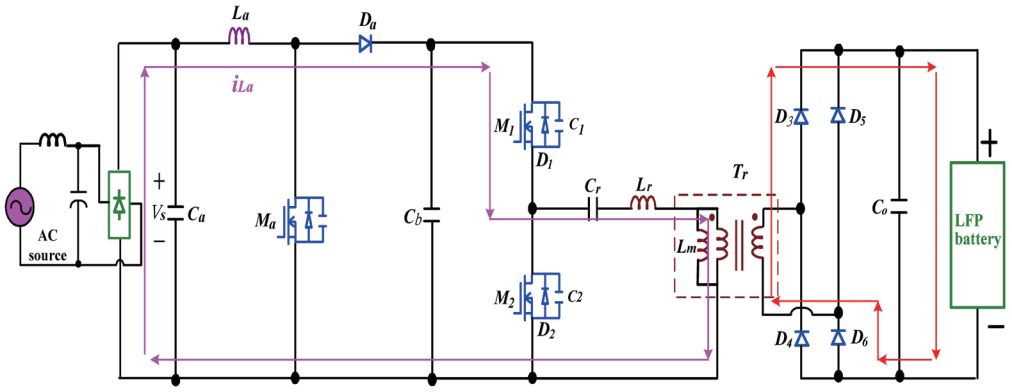

Fig. 5. (Color online) Equivalent circuit of operational Mode 1.

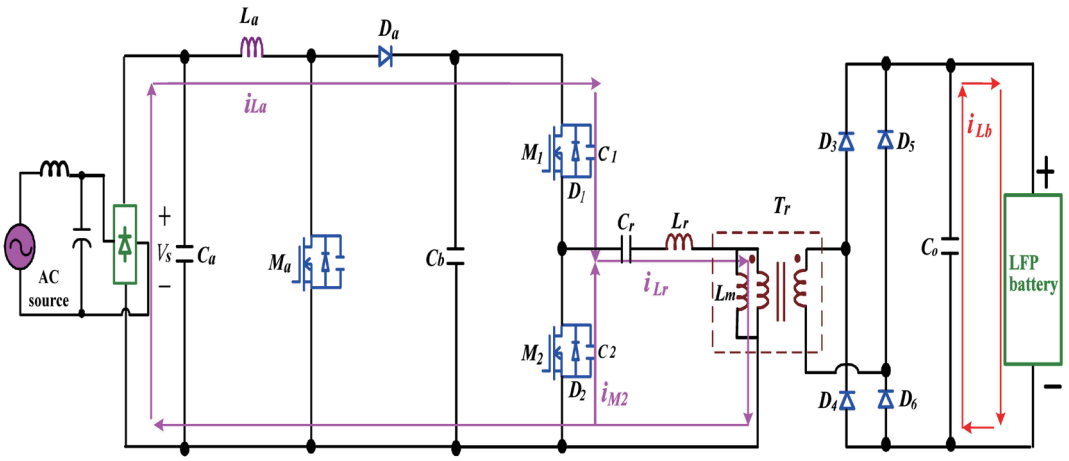

Fig. 6. (Color online) Equivalent circuit of operational Mode 2.

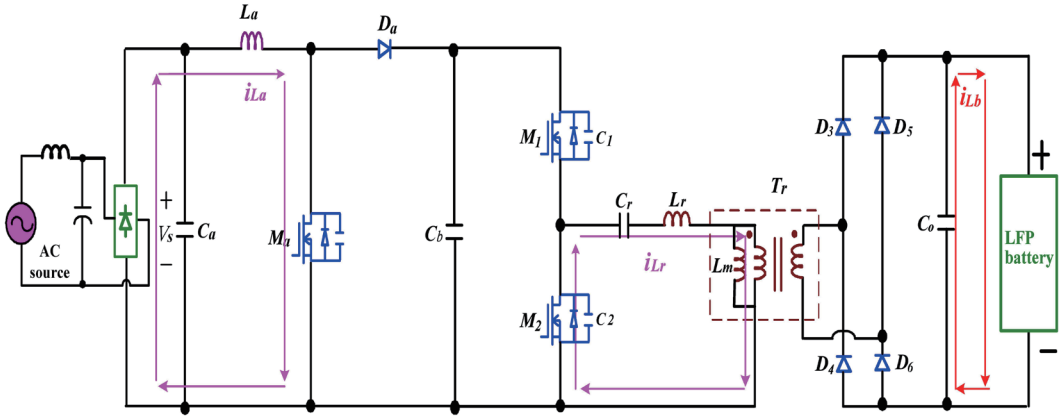

Fig. 7. (Color online) Equivalent circuit of operational Mode 3.

parasitic capacitance (C_2) voltage of the power switch (M_2) drops to zero and the power switch (M_1) is turned off. At this time, the resonant current i_{Lr} equals the current i_{M2} and the parasitic diode (D_2) of the power switch (M_2) is turned on. The resonant current i_{M2} is flowing through the path $Cr \rightarrow Lr \rightarrow L_m \rightarrow D_2$. In the secondary side of the transformer (T_r), the power diodes (D_3, D_4, D_5, and D_6) are continuously turned off and the current i_{Lb} is flowing through the path $C_o \rightarrow LFP$ battery. Figure 7 shows the equivalent circuit of the operational Mode 3.

2.4 Operational Mode 4

When the power switch (M_a) of the AC/DC charger is continuously turned on, the current i_{La} of the inductor is linearly increased, and the power switch (M_2) is turned on with a zero-voltage switching (ZVS) feature. The resonant current i_{Lr} is flowing through the path $Lr \rightarrow Cr \rightarrow M_2 \rightarrow L_m$. In the secondary side of the transformer (T_r), the diodes (D_4 and D_5) are switched on and the

power diodes (D_3 and D_6) are switched off. The current i_{Lb} is flowing through the path D_5→*LFP* battery→D_4. Figure 8 shows the equivalent circuit of the operational Mode 4.

2.5 Operational Mode 5

When the power switch (M_a) of the AC/DC charger is continuously turned on, the current i_{La} of the inductor is linearly increased. When the power switch (M_2) is turned off, the parasitic capacitance (C_2) of the power switch (M_2) is charged and the parasitic capacitance (C_1) of the power switch (M_1) is discharged. The resonant current i_{Lr} is revised, which divides into two paths. One is L_r→C_r→M_2→L_m and the other is L_r→C_r→M_1→C_b→L_m. In the secondary side of the transformer (T_r), the power diodes (D_4 and D_5) are switched on and the power diodes (D_3 and D_6) are switched off. The current i_{Lb} is flowing through the path D_5→*LFP* battery→D_4. Figure 9 shows the equivalent circuit of the operational Mode 5.

2.6 Operational Mode 6

When the power switch (M_a) of the AC/DC charger is continuously turned on and the current i_{La} of the inductor is linearly reduced, the parasitic capacitance (C_1) voltage of the active switch (M_1) drops to zero and the power switch (M_2) is turned off. At this time, the resonant current i_{Lr}

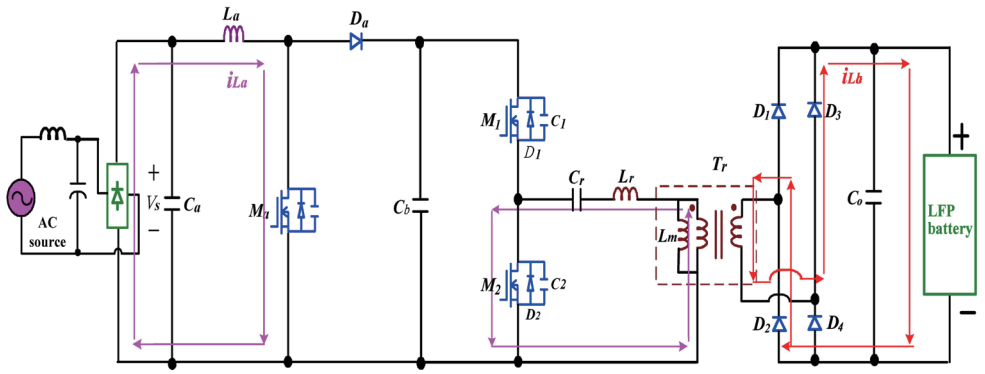

Fig. 8. (Color online) Equivalent circuit of operational Mode 4.

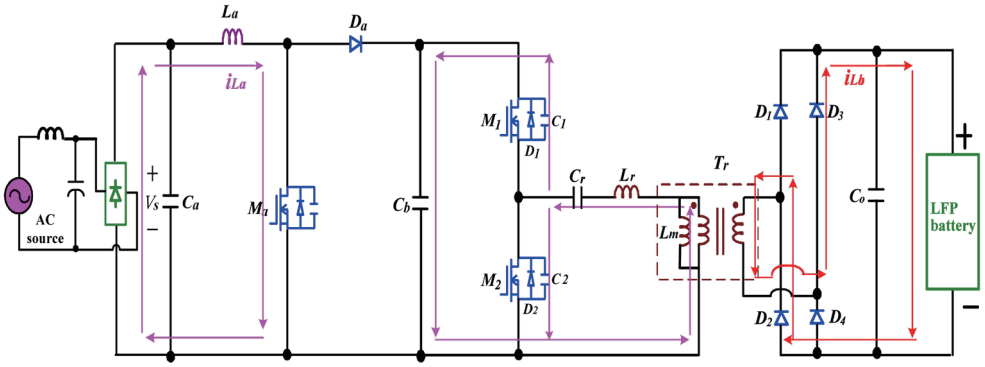

Fig. 9. (Color online) Equivalent circuit of operational Mode 5.

equals the current i_{M1} and the parasitic diode (D_1) of the power switch (M_1) is turned on. The resonant current i_{M1} is flowing through the path $C_r \rightarrow D_1 \rightarrow C_b \rightarrow L_m \rightarrow L_r$. In the secondary side of the transformer (T_r), the power diodes (D_4 and D_5) are turned on and the power diodes (D_3 and D_6) are turned off. The current i_{Lb} is flowing through the path $D_5 \rightarrow LFP$ battery$\rightarrow D_4 \rightarrow T_r$. Figure 10 shows the equivalent circuit of the operational Mode 6.

2.7 Operational Mode 7

When the power switch (M_a) of the AC/DC charger is turned off and the current i_{La} of the inductor is linearly decreased, the power switch (M_1) is switched on with a ZVS feature. The current i_{La} is flowing through the path $V_s \rightarrow L_a \rightarrow D_a \rightarrow C_b \rightarrow L_m$ and the resonant current i_{Lr} is flowing through the path $L_r \rightarrow C_r \rightarrow M_1 \rightarrow C_b \rightarrow L_m$. In the secondary side of the transformer (T_r), the power diodes (D_3, D_4, D_5, and D_6) are turned off. The current i_{Lb} is flowing through the path $C_o \rightarrow LFP$ battery. The operational mode of the AC/DC charger with high power factor and high efficiency over one switching cycle is completed. Figure 11 shows the equivalent circuit of the operational Mode 7.

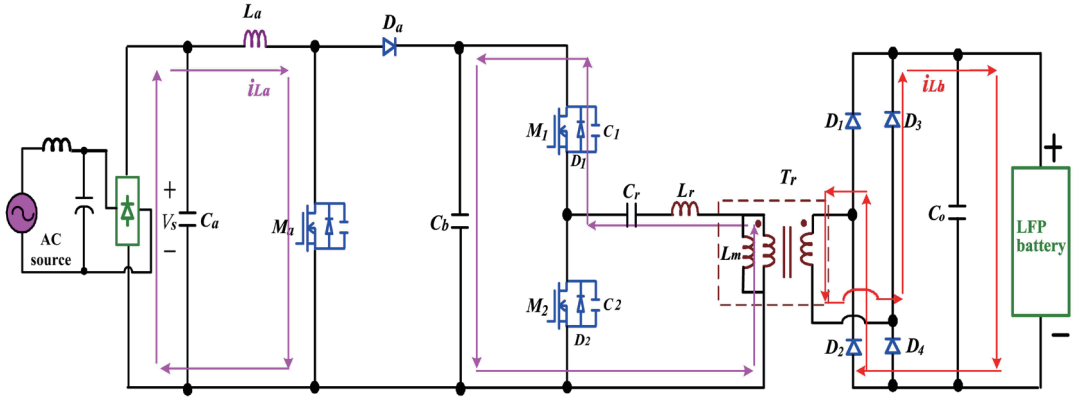

Fig. 10. (Color online) Equivalent circuit of operational Mode 6.

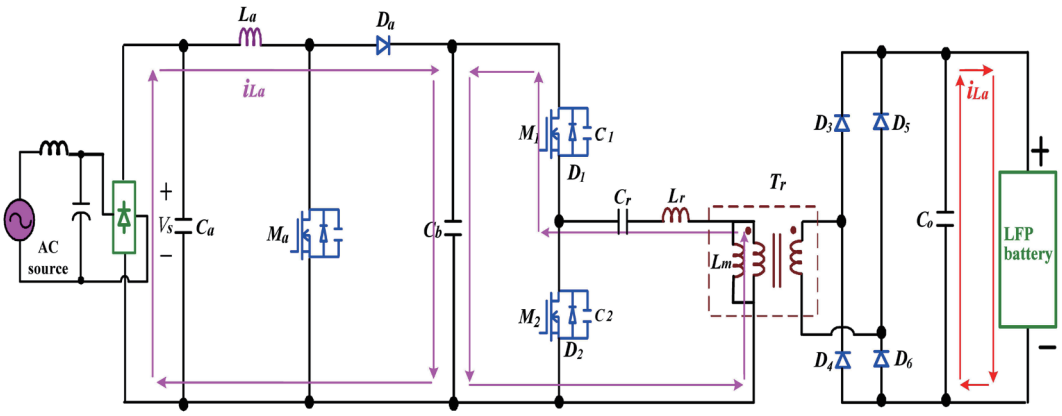

Fig. 11. (Color online) Equivalent circuit of operational Mode 7.

After the analysis of these operating modes, it can be seen that the AC/DC charger with features of high power factor and high efficiency can be verified.

3. Experimental Results

To confirm the function and probability of the AC/DC charger, a 240 W prototype of the AC/DC charger with high power factor and high efficiency is built. The AC/DC charger has the following specifications:

Input AC voltages: V_{AC} = 85–265 V_{rms},
Output DC voltage: V_o = 24 V_{DC},
Output current: I_o = 10 A,
Total output power: P_o = 240 W, and
Switching frequency of power switches: f = 100 kHz.

Figure 12 shows the experimental input voltage and current waveforms of the AC source. As determined using power quality analyzers, the experimental power factors are 0.996 and 0.966 under AC input voltages of 110 and 220 V_{rms}, respectively. Therefore, a high power factor of the proposed AC/DC charger can be obtained. Figure 13 shows the experimental waveforms of the output current change. When output currents change from 5 to 8 A, the output voltages are stable. Therefore, the load dynamic response of the AC/DC charger is achievable. Figures 14 and 15 show the results of efficiency measurements of the AC/DC charger with high power factor and high efficiency under full load conditions, from which the maximum efficiency can be as high as 96% at the AC input voltage of 220 V_{rms}.

(a)

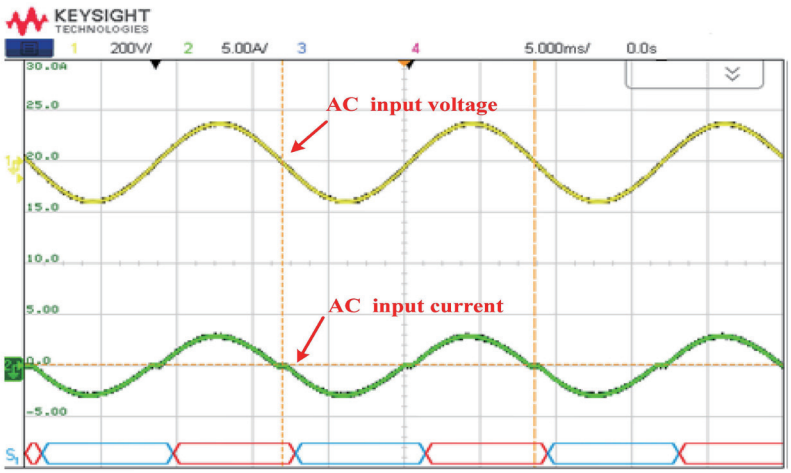

Fig. 12. (Color online) Experimental input voltage and current waveforms of AC source: (a) input voltage of 110 V_{rms}.

(b)

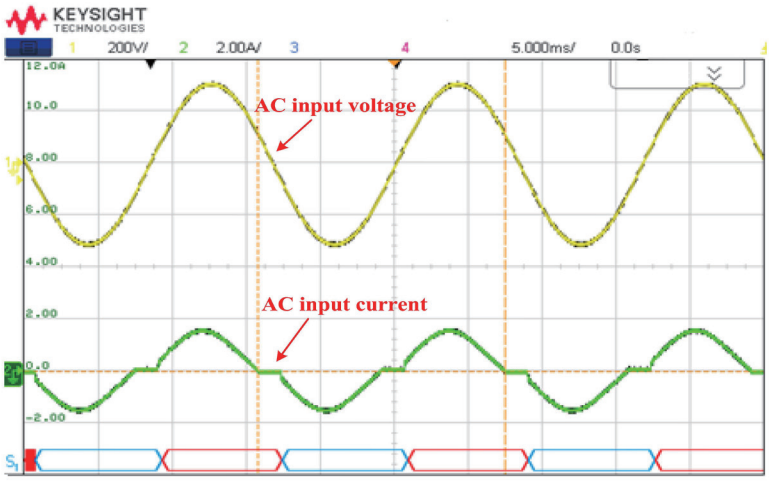

Fig. 12. (Continued) (Color online) Experimental input voltage and current waveforms of AC source: (b) input voltage of 220 V_{rms}.

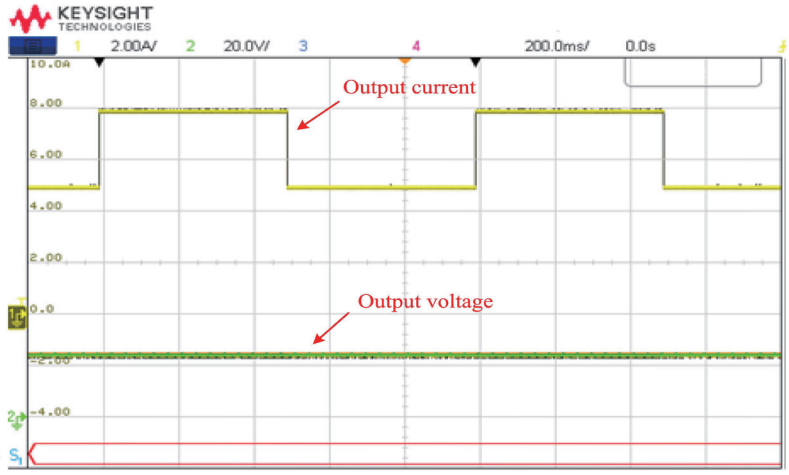

Fig. 13. (Color online) Experimental waveforms of output current change from 5 to 8 A.

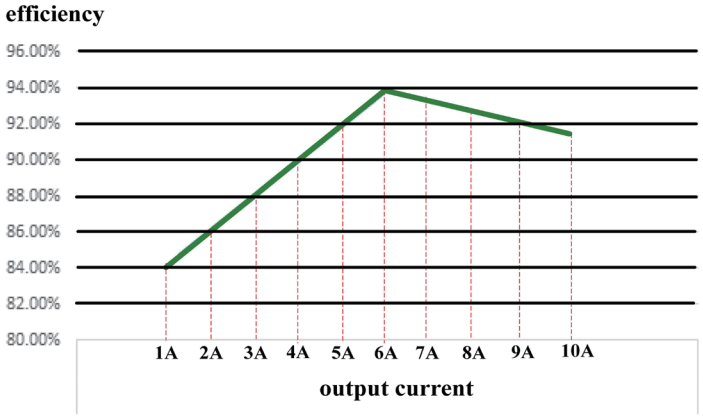

Fig. 14. (Color online) Plot of efficiency versus output current for AC/DC charger at AC input voltage of 110 V_{rms}.

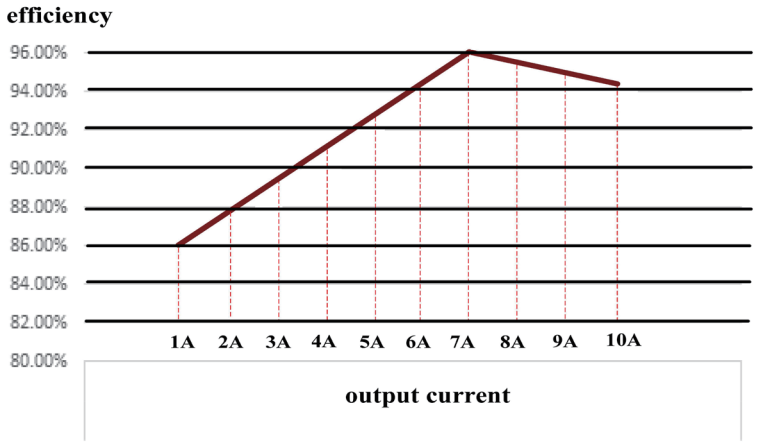

Fig. 15. (Color online) Plot of efficiency versus output current for AC/DC charger at AC input voltage of 220 V_{rms}.

4. Conclusions

In this study, the AC/DC charger with high power factor and high efficiency was built and implemented. It uses an active PFC circuit to decrease harmonic currents and increase the power factor, and it uses a DC/DC half- bridge LLC resonant converter to implement ZVS features of the power switches. Thus, the power losses of the power switches can be decreased and the efficiency of the AC/DC charger can be improved significantly. The results of the experiments have confirmed that the AC/DC charger with high power factor and high efficiency is relatively suitable for LFP batteries.

Author Contributions

Cheng-Tao Tsai designed and analyzed the circuit and wrote the paper. Feng-Wei Peng tested the circuit and analyzed the experimental results.

Conflicts of Interest

The authors declare no conflicts of interest.

References

1 M. Pavlovsky, G. Guidi, and A. Kawamura: IEEE Trans. Power Electron. **29** (2014) 851. https://doi.org/10.1109/TPEL.2013.2258358
2 C. M. Wang: IEEE Trans. Ind. Electron. **33** (2006) 768. https://doi.org/10.1109/TIE.2007.911917
3 H. Wang, H.-S. Chung, and A. Ioinovici: IEEE Trans. Power Electron. **27** (2012) 2242. https://doi.org/10.1109/TPEL.2011.2173588
4 B. Francesco, H. Weijian, and L. Corradini: IEEE Trans. Power Electron. **33** (2018) 9963. https://doi.org/10.1109/TPEL.2018.2796141

5 S. M. Chen, T. J. Liang, L. S. Yang, and J. F. Chen: IEEE Trans. Power Electron. **26** (2011) 1146. https://doi.org/10.1109/TPEL.2010.2090362
6 S. S. Dobakhshari, S. H. Fathi, and M. Jedari: IET Trans. Power Electron. **8** (2017) 607. https://doi.org/10.1109/IECON.2017.8216106
7 M. R. Mohammadi and H. Farzanehfard: IEEE Trans. Ind. Electron. **62** (2015) 1471. http://doi.org/10.1109/TIE.2014.2363425
8 B. Su, J. Zhang, and Z. Lu: IEEE Trans. Power Electron. **26** (2011) 427. https://doi.org/10.1109/TPEL.2010.2059046
9 C. A. Gallo, F. L. Tofoli, and J. A. C. Pinto: IEEE Trans. Power Electron. **25** (2010) 775. https://doi.org/10.1109/TPEL.2009.2033063
10 B. Lu, W. Liu, Y. Liang, F. C. Lee, and J. D. V. Wyk: 21st Annu. IEEE Applied Power Electronics Conf. and Expos. (APEC, 2006) 533−538. https://doi.org/10.1109/APEC.2006.1620590
11 B. Yang, F. C Lee, A. J. Zhang, and G. Huang: 18th Annu. IEEE Applied Power Electronics Conf. and Expos. (APEC, 2002) 1108−1112. https://doi.org/10.1109/APEC.2002.989382
12 B. Yang, F. C. Lee, and M. Concannon: 17th Annu. IEEE Applied Power Electronics Conf. and Expos. (APEC, 2003) 605−609. https://doi.org/10.1109/APEC.2003.1179276
13 B. Yang, C. H. Liang, T. J. Chen, K. H. Li, and J. S. Lee: 1st Int. Future Energy Electronics Conf. (IFEEC, 2013) 155−160. https://doi.org/10.1109/IFEEC.2013.6687496
14 R. J. Wai, C. Y. Lin, R. Y. Duan, and Y. R. Chang: IEEE Trans. Power Electron. **54** (2007) 354. https://doi.org/10.1109/TIE.2006.888794
15 H. Wang, S.-H. Chung, and A. Ioinovici: IEEE Trans. Power Electron. **27** (2012) 2242. https://doi.ogr/10.1109/TPEL.2011.2173588
16 Y. Park, B. Jung, and S. Choi: IEEE Trans. Power Electron. **27** (2012) 3568. https://doi.org/10.1109/TPEL.2012.2187342